

Simultaneous measurement of rheological properties in a microfluidic rheometer

Cite as: Phys. Fluids **32**, 052001 (2020); <https://doi.org/10.1063/5.0006060>

Submitted: 27 February 2020 . Accepted: 10 April 2020 . Published Online: 01 May 2020

Francesco Del Giudice 



View Online



Export Citation



CrossMark

ARTICLES YOU MAY BE INTERESTED IN

[Asymmetric flows of complex fluids past confined cylinders: A comprehensive numerical study with experimental validation](#)


Physics of Fluids **32**, 053103 (2020); <https://doi.org/10.1063/5.0008783>

[Influence of glow discharge on evolution of disturbance in a hypersonic boundary layer: The effect of first mode](#)

Physics of Fluids **32**, 051701 (2020); <https://doi.org/10.1063/5.0008457>


[On coughing and airborne droplet transmission to humans](#)

Physics of Fluids **32**, 053310 (2020); <https://doi.org/10.1063/5.0011960>



NEW!

Sign up for topic alerts
New articles delivered to your inbox



Simultaneous measurement of rheological properties in a microfluidic rheometer

Cite as: Phys. Fluids 32, 052001 (2020); doi: 10.1063/5.0006060

Submitted: 27 February 2020 • Accepted: 10 April 2020 •

Published Online: 1 May 2020



View Online



Export Citation



CrossMark

Francesco Del Giudice^{a)} 

AFFILIATIONS

System and Process Engineering Centre, Swansea University, Fabian Way, SA1 8EN Swansea, United Kingdom

^{a)} Author to whom correspondence should be addressed: francesco.delgiudice@swansea.ac.uk

ABSTRACT

Microfluidic rheometry is considered to be a potential alternative to conventional rheometry for the rheological characterization of viscoelastic solutions having relatively low viscoelastic properties. None of the microfluidic platforms introduced so far, however, can be used for the measurements of multiple rheological properties in the same device. In this work, I present the first microfluidic platform, named the “ μ -rheometer,” which allows for the simultaneous measurement of zero-shear viscosity η_0 and longest shear relaxation time λ . This is achieved by transforming the original “flow rate controlled” platform presented by Del Giudice *et al.*, “Rheometry-on-a-chip: Measuring the relaxation time of a viscoelastic liquid through particle migration in microchannel flows,” Lab Chip 15, 783–792 (2015) into a “pressure drop controlled” microfluidic device, by replacing a syringe pump with a pressure pump. The novel device has been tested by measuring both η_0 and λ for a number of polyethylene oxide solutions in glycerol–water 25 wt. % and pure water, respectively. Its effectiveness has been corroborated by means of a direct comparison with a conventional rotational rheometer.

© 2020 Author(s). All article content, except where otherwise noted, is licensed under a Creative Commons Attribution (CC BY) license (<http://creativecommons.org/licenses/by/4.0/>). <https://doi.org/10.1063/5.0006060>

I. INTRODUCTION

The rheological characterization of complex fluids is extremely important in a variety of fields, including the food industry,¹ cosmetics,² and biomedical engineering.^{3–5} Among the plethora of rheological properties of interest, the zero-shear viscosity η_0 and the longest relaxation time λ occupy a special place. Variations of η_0 in blood have been related to inflammatory or vascular diseases,^{5,6} similarly, variations of η_0 in food products have been associated with the change in perception of both sweetness and aroma.⁷ The longest relaxation time, instead, is a measure of the fluid elasticity, a critical parameter in many applications including coating,⁸ drag reduction,⁹ droplet formation,¹⁰ and mixing.¹¹ The accurate evaluation of the longest relaxation time is also very important for the design of microfluidic flow cytometers^{12–14} and for the design of cell and particle separation microfluidic devices.^{15,16} For the majority of applications listed above, values of zero-shear viscosity η_0 and longest relaxation time λ are generally small, with η_0 varying in the range of $1 < \eta_0/\eta_s < 10$, where η_s is the solvent viscosity, and λ varying in the range of $0.1 < \lambda < 100$ ms. While conventional bulk rheometry still allows for the measurement of small fluid viscosity values with

good accuracy, the same is not true for the longest relaxation time, which is often too small to be measured through conventional techniques.^{17–19} In the case of biological fluids, even the measurement of η_0 through conventional rheometry is sometimes not possible, as a bulk rheometer requires a large amount of samples (on the order of milliliters), and the measurement itself can be affected by edge-effects,²⁰ particularly evident in dilute biological solutions. Some of these limitations have previously been addressed by using *microrheology* techniques, where the Brownian motion of an ensemble of particles suspended in a polymer solution was tracked as a function of time in order to obtain their mean square displacement.²¹ By further using the Fourier transform on the data, it was possible to derive the frequency response of the solution.²² This approach still presents some challenges associated with the experimental setup, data analysis, and statistical significance. In an attempt to improve the effectiveness of microrheology techniques, it was demonstrated that the frequency response of a polymer solution could be obtained by tracking a single particle caged in an optical trap.^{23,24} This approach improved the statistical significance and reduced the statistical noise. However, rheological characterization via optical tweezers requires light-sensitive particles with a refractive index different from that

of the solution under investigation, a condition not always easy to fulfill.

To overcome the limitations associated with both conventional rheometry and microrheology, there has been significant interest in the so-called *microfluidic rheometry*.^{19,25,26} As suggested by the term, microfluidic rheometry employs microfluidic devices in order to derive rheological properties. Microfluidic devices present several advantages over conventional techniques: they require a small amount of samples, they are closed systems (no edge effects), and they can be easily integrated with other devices.¹⁹ So far, the majority of existing microfluidic rheometry platforms focused on the measurement of shear and extensional viscosity over a wide range of shear-rates. Hudson *et al.*⁴ employed a microfluidic rheometer to measure the shear viscosity of several polyethylene oxide and protein solutions up to imposed shear rate values of $\dot{\gamma} \sim 10^4 \text{ s}^{-1}$. Choi and Park⁵ employed a microfluidic device based on the co-flow between a reference fluid and the investigated fluid to measure the zero-shear viscosity of several protein solutions. Arosio *et al.*²⁷ designed a microfluidic device to evaluate the zero-shear viscosity of several protein solutions. Lee *et al.*²⁸ introduced a novel electrofluidic device for the measurement of zero-shear viscosity of xanthan gum and whole blood at different temperatures. Vishwanathan and Juarez²⁹ reported a probe-free technique for the measurement of the shear viscosity of Newtonian liquids by utilizing sub-kilohertz liquid oscillation frequencies around a cylindrical obstacle in a microfluidic device. Very recently, Gupta and Vanapalli³⁰ measured the shear-rheology of Newtonian and polyethylene oxide solutions in microchannel flows using the 3D-resolved flow kinematics obtained from digital holography microscopy. Several microfluidic platforms for the measurement of the extensional viscosity have also been introduced.²⁶ For instance, Hsiao *et al.*³¹ employed the “Stokes trap”³² to confine the 2D plane single micrometer-sized particles near the stagnation point of a planar extensional flow. Due to normal stresses, the particles migrated in the vertical toward the walls. The authors tracked the particle migration, and a second-order fluid model was developed for the extensional flow, which enabled the determination of extensional viscosity. Additional devices for the measurement of extensional viscosity can be found in the review by Haward.²⁶

While many platforms have been introduced for the measurement of shear viscosity,¹⁹ measurement of the longest *shear* relaxation time has been largely neglected (microfluidic techniques for the measurement of the *extensional* relaxation time can be found in the review by Haward²⁶). Zilz *et al.*¹⁷ were the first to introduce a microfluidic device for the estimation of the longest shear relaxation time. Their platform was based on the occurrence of elastic instabilities in curved geometries and was used to measure the longest relaxation time of dilute polyethylene oxide solutions. Koser *et al.*³³ designed a microfluidic device to measure the creep recovery of polyacrylamide solutions. By fitting the data to an existing theoretical model, Koser *et al.*³³ were able to evaluate the longest shear relaxation time. Del Giudice *et al.*¹⁸ introduced a methodology to measure the longest shear relaxation time of dilute and semi-dilute polymer solutions based on the transversal migration of particles suspended in polymer solutions flowing in a straight microchannel.^{34–36} The so-called μ -rheometer has been used for the evaluation of standard polyethylene oxide and polyacrylamide solutions,¹⁸ polyelectrolyte solutions (hyaluronic acid

and chitosan) with different sodium chloride concentrations,³⁷ atactic polystyrene solutions,³⁸ hydroxyethyl cellulose solutions,³⁹ and polymerized ionic liquid in ionic liquid solutions.⁴⁰ So far, however, no microfluidic rheometry platforms may be used for the measurement of multiple rheological properties; this is a significant limitation that prevents microfluidic rheometry from becoming the gold standard for the rheological characterization of polymer solutions, especially in dilute and semi-dilute polymer regimes where conventional rheometry fails due to technical and experimental limitations.⁴¹

In this work, the first microfluidic platform, called the μ -rheometer, for the simultaneous measurement of zero-shear viscosity η_0 and longest shear relaxation time λ is presented. The working principle of the μ -rheometer is the same as that introduced in the original publication,¹⁸ the only difference being that the flow is generated using a pressure pump instead of a syringe pump (Fig. 1). This modification allows for the simultaneous measurement of the zero-shear viscosity η_0 and the longest fluid relaxation time λ .

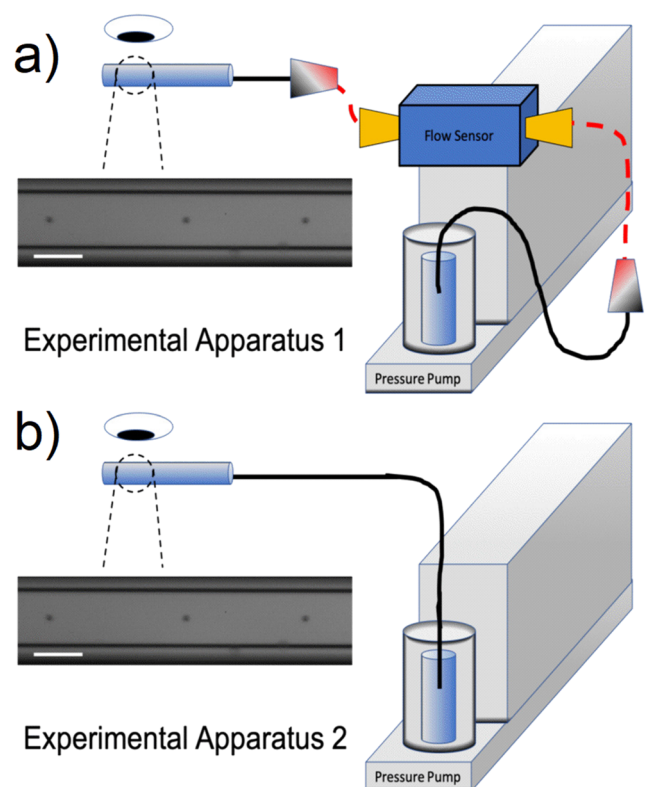


FIG. 1. Schematic representations of the two μ -rheometer apparatuses with (a) and without (b) the flow sensor. (a) The sample is inserted in the pressurized chamber of the pressure pump, and the pressure drop Δp is imposed. The suspension flows through the flow sensor first and then reaches the cylindrical microchannel, where videos of flowing particles are recorded. (b) The sample flows directly from the pressurized chamber into the cylindrical microchannel. Black solid lines represent tubes with an internal diameter $D_{i,connection} = 250 \mu\text{m}$ and an external diameter $D_{o,connection} = 1.6 \text{ mm}$. Red dashed lines represent tubes with an internal diameter $D_{i,sensor} = 400 \mu\text{m}$ and an external diameter $D_{o,sensor} = 1.6 \text{ mm}$. Scale bar in the snapshot is $100 \mu\text{m}$. Dimensions are not in scale.

This paper is organized as follows: Sec. II reports the theoretical background regarding the rheological behavior of dilute and semidilute unentangled polymer solutions, Sec. III reports the experimental setup, Sec. IV describes the working principle of the μ -rheometer, and Sec. V reports the comparison between the data measured using the μ -rheometer and those measured using conventional bulk rheology. Experimental data are also compared with available theoretical predictions. Advantages and limitations of the μ -rheometer setup are also discussed.

II. THEORETICAL BACKGROUND

The aim of this section is to provide the relevant background regarding the behavior of polymer solutions to better understand the results presented in Sec. V. When a polymer chain is added to a solvent, its configuration in solution depends on thermodynamic interactions occurring between the chain and the solvent molecules.⁴² One of the most common chain configurations in solutions is the random-coil, where the dimension of the coil (quantified by its hydrodynamic radius) depends upon the balance between two intramolecular interactions: the steric repulsion between monomers and the solvent-mediated attraction between monomers.⁴² These two interactions are perfectly balanced at a specific temperature called the θ -temperature (not to be confused with the parameter Θ introduced in Sec. IV). The solvent for the polymer at the θ temperature is called the theta (or θ) solvent. When the temperature $T > \theta$, the steric repulsion is stronger than the solvent-mediated attraction, thus leading to a coil with hydrodynamic radius larger than the one at $T = \theta$. In order to determine whether a solvent is a θ -solvent or a good solvent for a given polymer, the *dimensionless scaling exponent* ν was introduced. This parameter is related to the volume occupied by the random-coil in solution, with $\nu = 0.5$ for polymers in a theta-solvent and $\nu = 0.6$ for polymers in a good solvent.⁴² The conformation of the polymer in a solvent, however, does not necessarily need to fall in the category of good-solvent or θ -solvent: coils with different amounts of swelling can be found when the dimensionless scaling exponent falls in the range $0.5 < \nu < 0.6$.

Different chain conformations in solution result in marked differences in the macroscopic solution behavior, specifically, regarding the variation of both zero-shear viscosity η_0 and the longest relaxation time λ with the polymer concentration c . When the polymer concentration is far below the so-called overlapping concentration c^* (the concentration at which polymer chains start to interact), macroscopic rheological properties can be described through the Zimm model.⁴³ The scaling predictions that describe the variation of macroscopic rheological properties are generally presented in terms of specific viscosity at zero-shear $\eta_{sp,0} = \frac{\eta_0}{\eta_s} - 1$, where $\eta_{sp,0}$ is the zero-shear specific viscosity and η_s is the solvent viscosity. The specific viscosity represents the polymer contribution to the macroscopic dynamics of the solution. The scaling predictions for the specific viscosity $\eta_{sp,0}$ and the longest relaxation time λ in the dilute regime ($c \ll c^*$) are

$$\eta_{sp,0} \propto c \quad \text{and} \quad \lambda \propto c^0, \quad (1)$$

where λ is independent of the polymer concentration, as the polymer chains are assumed to be isolated and not interacting with the surrounding ones (an approximation valid for $c \ll c^*$).

The relaxation time in the dilute regime can be directly evaluated using the Zimm formula⁴³

$$\lambda_{\text{Zimm}} = \frac{F[\eta]M_w\eta_s}{RT}, \quad (2)$$

where $F = 1/\sum_{i=1}^N(1/i^{3\nu})$ is a parameter depending on the solvent quality (through the dimensionless scaling exponent ν), $[\eta] = \lim_{c \rightarrow 0} \frac{\eta_{sp,0}}{c}$ is the intrinsic viscosity of the polymer, M_w is the polymer molecular weight, $R = 8.314 \text{ J}/(\text{mol K})$ is the universal gas constant, and T is the absolute temperature.

When increasing the polymer concentration c near and above the overlapping concentration c^* , De Gennes⁴⁴ showed that the *correlation length* ξ (a measure of chain proximity^{42,45}) can be used to describe the dynamic of the solution in this new regime called *semidilute*. On scales smaller than ξ , monomers from the same chain are surrounded by solvent molecules,^{46–48} hydrodynamic interactions are not negligible, and the overall dynamic can be described via the Zimm model.⁴³ On scales larger than ξ , polymer chains interact with each other and hydrodynamic interactions are screened as a result of the presence of other chains.^{46–48} Therefore, polymer chains adopt a conformation of random walks of correlation blobs with size ξ . In these conditions, the solution dynamic is well described by the Rouse model,⁴⁹ with scaling predictions

$$\eta_{sp,0} \propto c^{1/(3\nu-1)} \quad \text{and} \quad \lambda \propto c^{(2-3\nu)/(3\nu-1)}, \quad (3)$$

which are valid in the *semidilute unentangled* regime where polymer chains interact without forming entanglements. At higher concentrations, polymer chains do entangle and the predictions become different from those of Eq. (3). The scaling predictions in the entangled polymer regime are not relevant for the present work, but they can be found in the manuscript by Colby.⁴⁵

III. MATERIALS AND METHODS

A. Material and preparation

Polyethylene oxide (PEO, Sigma Aldrich UK) with molecular weight $M_w = 4 \text{ MDA}$ in both glycerol–water 25 wt. % (hereafter labeled PG4) and pure aqueous solutions (hereafter labeled P4) at different mass concentrations in the range of $0.0398 < c < 0.7 \text{ wt. \%}$ was employed in this study. A PEO solution at a concentration of $c = 0.7 \text{ wt. \%}$ was prepared by direct addition of the polymer powder to both solvents. The other solutions were prepared by dilution of the stock using Gilson pipettes and a scale with 0.1 mg precision (Ohaus Adventurer Precision Balances).

For the microfluidic measurements in the μ -rheometer, the addition of particles was required (see Sec. IV for more details). Polystyrene particles (Polysciences, Inc.) with density $\rho_p = 1.05 \text{ g/l}$ and diameters $d_p = 15 \pm 1.5 \mu\text{m}$, $d_p = 10 \pm 1 \mu\text{m}$, and $d_p = 6 \pm 0.6 \mu\text{m}$ were added to the solutions. Particles with different sizes were employed in order to keep the confinement ratio $\beta = d_p/D \approx 0.1$ ($\beta = 0.1$ for experiments in $150 \mu\text{m}$ and $100 \mu\text{m}$ channels, while $\beta = 0.12$ for experiments in $50 \mu\text{m}$ channels), where D is the diameter of the μ -rheometer, in all the experiments; this precaution was required to fulfill the assumptions of $\beta \approx 0.1$ underlying the theoretical model for the evaluation of the fluid relaxation time,¹⁸ as described in Sec. IV. Dilute suspensions with volume fraction $\varphi = 0.02 \text{ wt. \%}$ were prepared by direct addition of particles to the

polymer solution and by using a mixer (Fisher Scientific). The effect of the particle addition on the fluid rheology can be neglected at such small φ values.⁵⁰ The suspension was immersed for 1 min in an ultrasonic bath (Fisher Scientific) to remove air bubbles and destroy potential particle aggregates. This procedure was repeated before each experiment.

B. Bulk shear rheometry

The viscosity curves for all the polymer solutions investigated were evaluated using a stress-controlled TA instruments AR2000ex rheometer. An acrylic cone with 60 mm diameter and a cone angle of 1° was used together with a custom made solvent-trap to avoid fluid evaporation. The temperature was controlled by a Peltier system and kept at $T = 20^\circ\text{C}$ for the PG4 solutions and $T = 22^\circ\text{C}$ for the P4 solutions. Different temperatures for the rheological characterization of PG4 and P4 are being required to match the temperature of the rooms in which the microfluidic experiments were performed.

C. Microfluidic apparatus

Two experimental apparatuses for the μ -rheometer were employed (Fig. 1). The first apparatus [Fig. 1(a)] included a pressure pump (Mitos P-Pump, Dolomite Microfluidics) connected to a flow sensor (Mitos flow-sensor, Dolomite Microfluidics) and then connected to the glass cylindrical microchannels (VitroCom, UK). Glass microchannels were used instead of the commonly encountered PDMS devices to avoid deformation of the channel walls which, in turn, could affect the μ -rheometrical measurements.⁵¹ Channels with different internal diameters, namely, $D = 50\ \mu\text{m}$, $D = 100\ \mu\text{m}$, and $D = 150\ \mu\text{m}$, and length $L = 100\ \text{mm}$ were used to tune the range of validity of the μ -rheometer measurements.³⁷ Silicone tubes (black solid and red-dashed lines in Fig. 1) were used to connect the pressure pump to the flow sensor and then to the glass microchannel. The second apparatus [Fig. 1(b)], instead, included the pressure pump directly connected to the glass cylindrical microchannel. In both apparatuses, particles flowing in the microchannel (snapshots in Fig. 1) were observed using an inverted microscope (Zeiss Axiovert 135) in bright field with a $5\times$ objective (Zeiss Objective Epiplan $5\times/0.13\ \text{W}0.8$, $\text{WD} = 20.5\ \text{mm}$). The estimated depth of field for this objective is $\sim 60\ \mu\text{m}$. Therefore, choosing the channel centerline as the focal plane, particles were always in focus regardless of their position across the channel cross section. Images of flowing particles were recorded by using a fast camera (Photron, fastcam Mini UX50) at a frame rate between 50 fps and 8000 fps, depending on the imposed pressure drop in the range $60 < \Delta p < 500\ \text{mbar}$. All the microfluidic experiments were carried out at room temperature, measured using a digital room thermometer (Habor technology). Particles were tracked using a well established Interactive Data Language (IDL) (Harris Geospatial solutions) subroutine⁵² available online (<http://www.physics.emory.edu/faculty/weeks/idl/>) and used in the previous works.^{18,37,38} A minimum of 100 particles were tracked for each measurement at an imposed pressure drop Δp . Results from the particle tracking were subsequently analyzed to derive η_0 and λ by using a homemade Matlab code. The values of zero-shear viscosity η_0 and the longest relaxation time λ were derived as the average of two or three independent measurements taken at different imposed pressure drops Δp .

IV. WORKING PRINCIPLE OF THE μ -RHEOMETER

The working principle of the μ -rheometer employed in this work is the same as that introduced in the original publication,¹⁸ with the only difference being that the flow here is generated using a pressure pump instead of syringe pumps (Fig. 1). This modification allows for the simultaneous measurement of the zero-shear viscosity η_0 and the longest fluid relaxation time λ . The phenomenon underlying the working principle of the μ -rheometer is the centerline transversal migration of particles suspended in polymer solutions with nearly constant viscosity flowing in microfluidic channels.^{34–36,53} When shear-thinning features are not negligible and when the confinement ratio $\beta \leq 0.1$, particles migrate toward the walls of a straight channel.^{54–56} Under a practical point of view, this means that if, during the experiments, particles attain equilibrium positions near the walls of a straight channel, the μ -rheometer cannot be used.

A. Measurement of the zero-shear viscosity

It is well-known that for fluids having a constant viscosity value within the range of explored shear rates, whether they are Newtonian or non-Newtonian, their bulk flow in straight channels can be described by the Hagen–Poiseuille law that relates the pressure drop to the flow rate as⁵⁷

$$\Delta p = \frac{128\eta_0 QL}{\pi D^4} = \eta_0 Q \mathcal{R}, \quad (4)$$

where Δp is the imposed pressure drop, η_0 is the zero-shear viscosity (i.e., the constant viscosity value in the low-shear plateau region of the flow curve), Q is the volumetric flow rate, D is the channel internal diameter, and L is the channel length. The symbol $\mathcal{R} = 128L/(\pi D^4)$ is the geometrical flow resistance and is here used to simplify the notation. Equation (4) is valid when the fluid presents a constant viscosity and when the pressure pump is directly connected to the channel with diameter D and length L . In this work, the microchannel was connected to the pressure pump by using a series of different tubes (Fig. 1); thus, Eq. (4) is not strictly valid. For a fluid with viscosity η_0 flowing with constant flow rate Q in a series of N cylindrical tubes, the overall pressure drop can be written as

$$\Delta p_{\text{tot}} = \sum_{i=1}^N \Delta p_i = \eta_0 Q \sum_{i=1}^N \mathcal{R}_i, \quad (5)$$

where \mathcal{R}_i is the geometrical flow resistance in each cylindrical tube with diameter D_i and length L_i . Note that, in Eq. (5), the localized viscous losses were neglected; this is a good approximation when the ratio $L/D \gg 1$, a condition always fulfilled in the experiments reported therein. Equation (5) can be rewritten in terms of zero-shear viscosity η_0 as

$$\eta_0 = \frac{\Delta p_{\text{tot}}}{Q \sum_{i=1}^N \mathcal{R}_i}, \quad (6)$$

which is required for the evaluation of the zero-shear viscosity. The pressure drop Δp is imposed in every experiment and, therefore, is a known quantity; the geometrical flow resistance $\mathcal{R} = \sum_{i=1}^N \mathcal{R}_i$ is also known as it depends on the employed tube dimensions. The volumetric flow rate Q can be either measured through the flow sensor [experimental apparatus of Fig. 1(a)] or from the tracking of the particles flowing on the centerline of the microchannel

(snapshots in Fig. 1). For this second approach to be accurate within 0.6% of error, Higdon and Muldowney⁵⁸ reported that the confinement ratio β defined as the ratio between the particle diameter d_p and the channel diameter D should be $\beta = d_p/D \sim 0.1$ or smaller; this condition was always fulfilled in the experiments reported herein. Particles flowing at the centerline display the largest possible velocity due to the parabolic velocity profile in cylindrical microchannels. The relation between the maximum and the average fluid velocity in circular pipes is⁵⁷ $v_{max}/\bar{v} = 2$. From the average velocity \bar{v} , the flow rate is evaluated as $Q = \bar{v}\pi D^2/4$. This approach was found to be accurate (Fig. 2). It is clear from Eq. (6) that a precise estimate of the flow resistance \mathcal{R}_i is important to accurately measure the zero-shear viscosity η_0 . In practical terms, the diameter of the microchannel is either provided by the manufacturer or measured after fabrication. An error of 5% in the measurement of D (this is a conservative estimate) can lead to an error in the evaluation of \mathcal{R} of $\sim 20\%$, which, in turn, will lead to a value of η_0 carrying an error up to 20%, depending on the number of flow resistances \mathcal{R}_i affected. The error committed when measuring the channel length L can be roughly of 1 mm or less over a tube length of 10 cm or more, which is 10% or less.

In summary, the zero-shear viscosity can be evaluated by using any of the two experimental apparatus of Fig. 1 and by employing Eq. (6). Note that, no calibration is required to calculate the zero-shear viscosity, as the geometrical flow resistance is known *a priori*, and all the localized viscous losses have been neglected (the validity of this last assumption is confirmed by the good agreement observed between the data of Fig. 2).

B. Measurement of the longest relaxation time

Particles suspended in a near constant-viscosity non-Newtonian fluid flowing in a microfluidic channel experience an elastic force

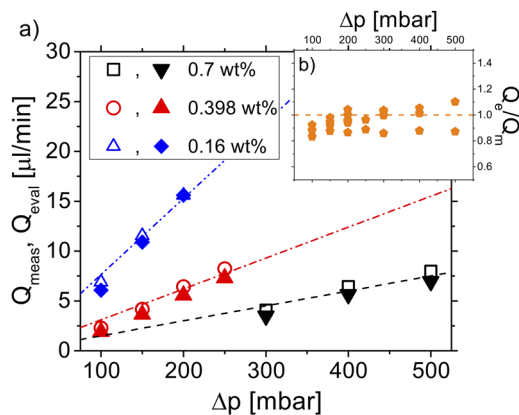


FIG. 2. (a) Good agreement between the flow rate values measured at different imposed pressure drops Δp using the flow sensor, Q_{meas} (open symbols), and those estimated through the particle tracking, Q_{eval} (closed symbols), is observed for several PEO in glycerol–water solutions. The diameter of the suspended particles is $d_p = 15 \mu\text{m}$, while that of the channel is $D = 150 \mu\text{m}$ (confinement ratio $\beta = d_p/D = 0.1$). Different symbols represent different polymer concentrations. The inset (b) shows that the ratio between the evaluated and the measured flow rate is $Q_e/Q_m \approx 1$ in the whole range of Δp investigated.

that drives transversal migration toward the middle plane of the channel cross section.³⁴ When the cross section is either square-shaped or circular, particles migrate toward the channel centerline.^{35,36,53} Romeo *et al.*⁵⁹ introduced a relation between the normalized fraction of particles aligned on the centerline due to the elasticity of the suspending fluids, f_1 , and the dimensionless parameter $\Theta = De(L_z/D)\beta^2$, where L_z is the distance from the channel inlet at which the particles are observed (which is different from the total channel length L), D is the microchannel diameter, and $\beta = d_p/D$ is the confinement ratio, with d_p being the particle diameter. The symbol De indicates the Deborah number, defined as $De = 4\lambda Q/(\pi D^3)$, where λ is the longest relaxation time and Q is the volumetric flow rate. The theoretical relation found by Romeo *et al.*⁵⁹ can be expressed in analytical form as¹⁸

$$f_1 = \frac{1}{1 + Be^{-C\Theta^2}}, \quad (7)$$

where $B = 2.7$ and $C = 2.75$ are constants derived from the best fit of the data by Romeo *et al.*⁵⁹ The normalized fraction of particles aligned on the centerline, f_1 , is derived after dividing the channel cross section into $k = 6$ circular fluid bands, and it can be evaluated as

$$f_1 = \frac{\frac{n_1}{A_1 \bar{v}_1}}{\sum_{k=1}^6 \frac{n_k}{A_k \bar{v}_k}}, \quad (8)$$

where the subscript k indicates the fluid cross-sectional band, A_k is the area of the k th band, and \bar{v}_k is the average velocity of the fluid enclosed in the band k . The number of bands k was fixed equal to $k = 6$ in the original publication,¹⁸ and particles were assigned to each band through the evaluation of the ratio between the velocity of each particle V_p and the maximum particle velocity observed $V_{p,max}$. The values of $V_p/V_{p,max}$, A_k , and \bar{v}_k are reported in Table I (retrieved from the original publication¹⁸), and they apply only when the confinement ratio is $\beta \sim 0.1$.

Equation (7) can be written in terms of the longest relaxation time as

$$\lambda = \kappa \frac{\pi}{4} \frac{1}{\beta^2} \frac{D^4}{LQ} \sqrt{\frac{1}{C} \ln\left(\frac{f_1 B}{1 - f_1}\right)}, \quad (9)$$

TABLE I. Numerical values of each band k (first column) required for the evaluation of the normalized fraction of particles f_1 [Eq. (7)] retrieved from Del Giudice *et al.*¹⁸ The values of the ratio between the particle velocity and the maximum particle velocity $V_p/V_{p,max}$ (second column), the areas A_k (third column), and the average fluid velocities \bar{v}_k (fourth column) are reported. The values of $V_p/V_{p,max}$ reflect the assumption that the particle velocity is the same as the fluid velocity, valid when the confinement ratio is $\beta \sim 0.1$ (see the main text for more information).

Band	$V_p/V_{p,max}$	A_k	\bar{v}_k
1	0.98	0.018	0.99
2	0.92	0.054	0.95
3	0.82	0.093	0.87
4	0.67	0.138	0.75
5	0.46	0.192	0.57
6	...	0.507	0.18

where $\kappa = 1$ when λ was measured in s/rad (as derived from the linear viscoelastic response with the angular frequency ω expressed in rad/s) or $\kappa = 2\pi$ when λ was measured in s. In this work, the value $\kappa = 1$ was employed. Equation (9) is valid when $\Theta \leq 1.4$ (f_1 is a very weak function of Θ for $\Theta > 1.4$), when $De < 1$, when inertial effects are negligible, and for confinement ratio values $\beta \sim 0.1$. Inertial effects are quantified by the Reynolds number $Re = \rho \bar{v} D / \eta$, where ρ is the fluid density, \bar{v} is the average fluid velocity [$\bar{v} = Q / (\pi D^2 / 4)$ for cylindrical channels], D is the channel diameter, and η is the shear viscosity. Inertial effects become relevant when the Reynolds number is⁶⁰ $Re = O(1)$. If any of the above mentioned conditions ($\Theta < 1.4$, $De < 1$, $Re < 1$, and $\beta \sim 0.1$) is not fulfilled, then the value of the relaxation time derived from Eq. (9) may not be accurate. Note that even the measurement of λ through Eq. (9) does not require a calibration curve, as the theoretical curve introduced by Romeo *et al.*⁵⁹ is a *universal master curve* valid as long as its underlying assumptions are fulfilled.

In summary, by tracking flowing particles, it is possible to evaluate the volumetric flow rate Q and the normalized fraction of particles aligned on the centerline f_1 . Once those two parameters are known, the zero-shear viscosity is evaluated through Eq. (6) and the longest relaxation time through Eq. (9). Since Q and f_1 can be identified from the analysis of the same dataset, it is possible to evaluate simultaneously both η_0 and λ without the need of any prior calibration.

V. RESULTS AND DISCUSSION

A. Rheological data

Polyethylene oxide dissolved in two different solvents, namely, glycerol–water 25 wt. % (PG4 solutions) and pure water (P4 solutions), were employed to prove the reliability of the μ -rheometer. In order to validate the values of η_0 and λ measured through the μ -rheometer, a standard rheological characterization of the solutions was carried out (Fig. 3). In good agreement with previous literature findings,^{61,62} PG4 solutions at concentration $c > 0.1$ wt. % exhibited a plateau region at low shear rate values followed by mild shear-thinning features above a critical value of the shear rate $\dot{\gamma}_c$ [Fig. 3(a)]. Below $c = 0.1$ wt. %, the viscosity was nearly constant over the whole range of the shear rate $\dot{\gamma}$ investigated. Similar observations could be made for the P4 solutions (Fig. 3). The clear distinction of behaviors above/below the concentration value $c = 0.1$ wt. % suggested the possibility that the overlap concentration was $c^* \sim 0.1$ wt. % for both fluids, thus implying that the quality of the solvent was similar for PG4 and P4. An independent estimate of the overlap concentration for both sets of solutions could be derived by rearranging the data of Figs. 3(a) and 3(b) in terms of reduced viscosity $\eta_{red} = \eta_{sp,0}/c$ [Fig. 3(c)].⁵⁰ The overlap concentration could be estimated as either $c^* = 1/[\eta]$ (Flory theory⁶³) or $c^* = 0.77/[\eta]$ (Gressley theory⁶⁴), where $[\eta] = \lim_{c \rightarrow 0} \eta_{red}$ is the intrinsic viscosity. From the data of Fig. 3(c), a value of intrinsic viscosity $[\eta]_{PG4} = 8.07$ dl/g for PG4 solutions and $[\eta]_{P4} = 9.70$ dl/g for P4 solutions was found. The estimated overlap concentrations according to the Flory theory were $c_{PG4}^* = 1/[\eta]_{PG4} = 0.12$ g/dl and $c_{P4}^* = 1/[\eta]_{P4} = 0.1$ g/dl. Both values could be compared to the theoretical prediction of $[\eta]$ from the Mark–Houwink relation⁶⁵ $[\eta]_{MH} = 0.072 M_w^{0.65} = 14.08$ g/dl, with an estimated overlap concentration of $c_{MH}^* = 0.07$ wt. %,

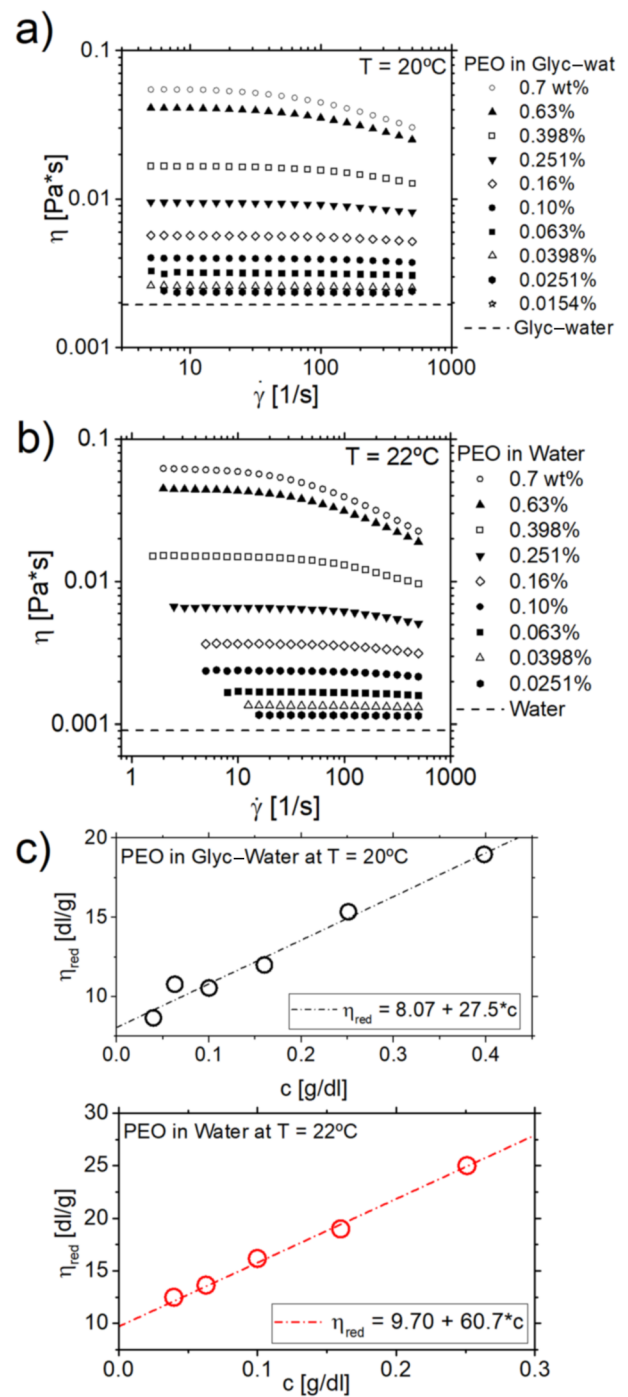


FIG. 3. Shear viscosity η as a function of the shear rate $\dot{\gamma}$ for PEO solutions in glycerol–water 25 wt. % at $T = 20^\circ\text{C}$ (a) and PEO solutions in pure water at $T = 22^\circ\text{C}$ (b). Dashed lines in (a) and (b) represent the measured solvent viscosity. (c) Reduced viscosity $\eta_{red} = \eta_{sp,0}/c$ as a function of the polymer concentration c for PEO in glycerol–water (top) and PEO in pure water (bottom). Dotted-dashed lines are the best linear fitting curves, which identify the intrinsic viscosity $[\eta] = \lim_{c \rightarrow 0} \eta_{red}$. For the PEO in glycerol–water (open black circles), $[\eta] = 8.07$ dl/g, while for PEO in water (open red circles), $[\eta] = 9.70$ dl/g.

in good agreement with the value $c^* \approx 0.1$ wt.% derived from the data of Fig. 3 and with the value $c^* = 0.1$ g/dl measured by Kang *et al.*⁶⁵

It is now time to present a comparison between the conventional bulk rheometry and the μ -rheometer data for PG4 solutions (Fig. 4). As anticipated in Sec. II, information regarding the dynamics of the polymer chains in solution can be derived from the analysis of the specific viscosity $\eta_{sp,0}$ as a function of the concentration c . A very good agreement was observed between the $\eta_{sp,0}$ data derived through conventional and microfluidic rheometry (Fig. 4). Red triangles in Fig. 4 were obtained by using experimental apparatus 1 [Fig. 1(a)], i.e., including a flow sensor, while the blue circles were obtained by using simpler (also cheaper) experimental apparatus 2 [Fig. 1(b)]. In both cases, the flow rate was measured by particle tracking. The data were well-described by a straight line $\eta_{sp,0} \propto c$ for $c < 0.1$ g/dl, in agreement with the theoretical predictions for the dilute regime [Eq. (1)]. For concentrations larger than $c = 0.1$ g/dl, the data were well described by the power law $\eta_{sp,0} \propto c^{1.58 \pm 0.11}$ obtained through the least squares minimization analysis.⁶⁶ By comparing the best fit exponent with the scaling prediction of Eq. (3), the dimensionless scaling exponent $\nu = 0.544$ was derived, in good agreement with the exponent $\nu = 0.55$ found by Tirtaatmadja *et al.*⁶³ on aqueous PEO solutions, thus suggesting that glycerol–water 25 wt. % is a relatively good solvent for the PEO at $T = 20^\circ\text{C}$. The different trend displayed by the data across $c = 0.1$ g/dl further strengthened the argument that the overlapping concentration for PG4 solutions analyzed in this work was $c^* = 0.1$ g/dl.

Simultaneously to the specific viscosity, it was possible to evaluate the longest relaxation time by using Eq. (9). The relaxation time data could not be measured using standard oscillatory shear measurements⁵⁰ as the rheometer torque detected during the experiments was very close to, or lower than, the limiting torque of the rheometer (data not shown). An estimate of the longest relaxation time was derived by fitting the viscosity curves of Fig. 3(a) with the Bird–Carreau model,⁵⁷

$$\eta = \eta_\infty + \frac{\eta_0 - \eta_\infty}{\left[1 + (\lambda\dot{\gamma})^2\right]^{\frac{1-n}{2}}}, \quad (10)$$

where η_0 is the zero-shear viscosity, $\eta_\infty = 0$ is the plateau viscosity at infinite shear, λ is the longest relaxation time, and n is the flow-index. The estimate of λ through Eq. (10) is based on the argument that the polymer chain in solution ceases to be a random coil across a critical shear rate value $\dot{\gamma}_c$ when the solutions start to display shear-thinning features; the longest relaxation time is estimated as $\lambda = 1/\dot{\gamma}_c$. Note that the experiments with the μ -rheometer were carried out by imposing a pressure drop such that the maximum shear rate in the glass microchannel $\dot{\gamma}_{max} = 8Q/(\pi D^3)$ was always smaller than the critical shear rate $\dot{\gamma}_c$. Therefore, the velocity profile in the microchannel was always parabolic and both the Hagen–Poiseuille law [Eq. (5)] and the relation of Romeo *et al.*⁵⁹ [Eq. (7)] were valid.

The data derived from the Bird–Carreau fitting were found to be in good agreement with those measured through the μ -rheometer above the overlap concentration c^* [Fig. 4(b)]. Below c^* , it was not possible to employ the Bird–Carreau model to estimate the relaxation time, as the viscosity curves for PG4 did not display any shear-thinning feature [Fig. 3(a)]. The experimental data of Fig. 4(b) were

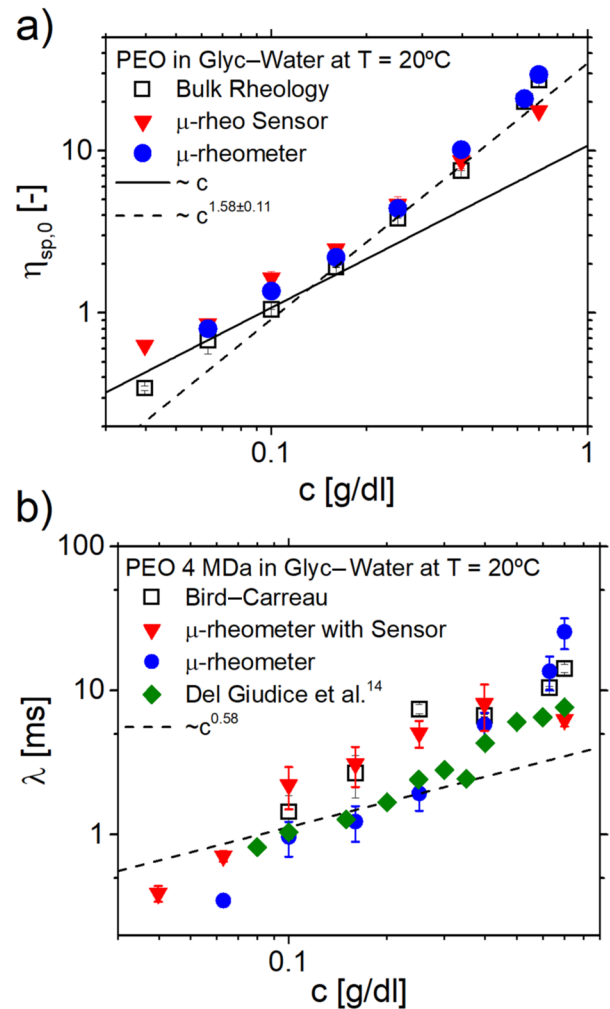


FIG. 4. Good agreement between the conventional rheometry data (open squares) and the μ -rheometer data (red triangles and blue circles) is observed. (a) Specific viscosity $\eta_{sp,0}$ as function of the polymer concentration c . Red triangles refer to the data derived through experimental apparatus 1 [Fig. 1(a)], while blue circles refer to the data derived through experimental apparatus 2 [Fig. 1(b)]. For red triangles, the internal diameter of the glass microchannel is $D = 150 \mu\text{m}$ for $c \geq 0.1$ g/dl and $D = 150 \mu\text{m}$ for $c < 0.1$ g/dl. For blue circles, the internal diameter of the μ -rheometer is $D = 100 \mu\text{m}$. No significant difference between the data can be observed. Dashed lines are the best fitting obtained through Eq. (3), while the solid line is Eq. (1). From the best fitting through Eq. (3), a value of $\nu = 0.544$ was obtained. (b) Longest relaxation time λ as a function of the polymer concentration c . Symbols are as in (a). Green diamonds are the data derived from the paper of Del Giudice *et al.*¹⁸ using the μ -rheometer with the flow rate controlled by using syringe pumps. The relaxation time for the conventional rheometry was estimated from the Bird–Carreau model⁵⁷ applied to the viscosity curve of Fig. 3(a). Dashed line is the theoretical prediction of Eq. (3) with $\nu = 0.544$ derived from the data in (a). Error bars falling within the symbol are not shown.

well described by the scaling law for the longest relaxation time in the semidilute unentangled regime [Eq. (3)], where the dimensionless scaling coefficient was set to $\nu = 0.544$, derived from the best fit of the viscosity data of Fig. 4(a). The relaxation time data were also

found to be in good agreement with those of Del Giudice *et al.*¹⁸ (green diamonds in Fig. 4) on PG4 solutions, measured using the μ -rheometer with the flow rate controlled by using syringe pumps. For the relaxation time, the tiny discrepancy observed between the μ -rheometer data measured with and without the flow sensor is minimal and, in general, falls near the experimental uncertainty (see the error bars).

An important conclusion that can be drawn for the data of Fig. 4 is that the flow sensor is not necessary for the simultaneous measurement of rheological properties, as the volumetric flow rate Q evaluated via the tracking of particles flowing at the centerline leads to an accurate estimate of the viscosity through Eq. (6). With this reasoning, rheological properties for P4 solutions were derived using experimental apparatus 2 [Fig. 1(b)] and were compared to the conventional rheology data (Fig. 5). For the viscosity data, good agreement was observed across all the concentrations [Fig. 5(a)]. The data above the overlap concentration $c^* = 0.1$ g/dl were well described by the power law $\eta_{sp,0} \propto c^{1.67 \pm 0.086}$, which returned a value of the dimensionless scaling exponent $\nu = 0.533$, again suggesting that water is a relatively good solvent for the PEO, in agreement with the literature.^{62,63} Relaxation time values derived from bulk rheology through the Bird–Carreau fitting of the viscosity curves were found to be in good agreement with μ -rheometer data for polymer concentrations $c > 0.2$ g/dl. For smaller polymer concentrations c , shear-thinning features were not clearly observable in the P4 viscosity curves [Fig. 3(b)], and the resulting estimate of the longest relaxation time λ was affected by large error bars (open squares). The data above c^* , derived through the μ -rheometer (blue circles), were also well described by the theoretical predictions of Eq. (3) with dimensionless scaling coefficient $\nu = 0.533$. For concentrations below the overlap concentrations, a plateau in the relaxation time values was observed, in agreement with the theoretical predictions of Eq. (1). The estimated Zimm relaxation time through Eq. (2) was $\lambda_{zimm} = 0.78$ ms, where $T = 295$ K, $[\eta] = 9.7$ dl/g, $M_w = 4$ MDa, $\eta_s = 9.04 \times 10^{-4}$ Pa s (measured through conventional bulk rheometry), and $F = 1/\sum_{i=1}^N (1/i^{3\nu}) = 0.542$, in good agreement with the μ -rheometer data for $c < c^*$.

B. Advantages and limitations of the μ -rheometer

The clear advantage of the μ -rheometer over the existing microfluidic techniques is the simultaneous measurement of zero-shear viscosity η_0 and longest relaxation time λ by using a volume of liquid as small as 100 μ l. The measurement of η_0 and λ for one polymer solution takes around 5 min, depending on the time required to stabilize the flow rate after imposing the pressure drop Δp . Incidentally, the flow in the microchannel stabilizes faster when using a pressure pump instead of a syringe pump (stabilization for 10 min or more due to the inertia of the syringes), which is an advantage in terms of time required to carry out the measurement. Existing microfluidic platforms have so far¹⁹ allowed for the measurement of either η_0 or λ . Even though the μ -rheometer cannot be used to derive a full viscosity curve, the evaluation of the zero-shear viscosity is, in general, sufficient to draw conclusions regarding the behavior of the polymer solutions. As reported in Sec. II, the scaling of polymer solutions experiencing distinct polymer–solvent interactions can be described by different scaling predictions obtainable through the evaluation of the dimensionless scaling exponent

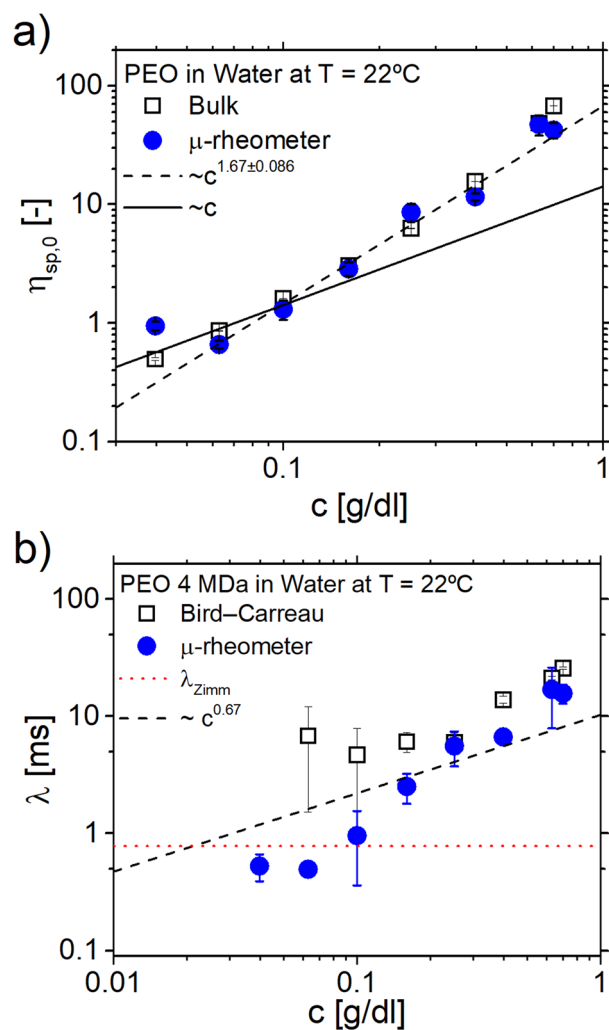


FIG. 5. Good agreement between the conventional rheometry data (open squares) and the μ -rheometer data (red triangles and blue circles) is observed. (a) Specific viscosity $\eta_{sp,0}$ as a function of the polymer concentration c . Blue circles refer to the data derived through experimental apparatus 2 [Fig. 1(b)]. Dashed lines are the best fitting obtained through Eq. (3), while the solid line is Eq. (1). From the best fitting through Eq. (3), a value of $\nu = 0.533$ was obtained. (b) Longest relaxation time λ as a function of the polymer concentration c . Symbols are as in (a). The relaxation time for the conventional rheometry was estimated from the Bird–Carreau model⁵⁷ applied to the viscosity curve of Fig. 3(b). A μ -rheometer with diameter $D = 100$ μ m was used for the measurements at $c \geq 0.1$ g/dl, while a μ -rheometer with diameter $D = 50$ μ m was used for the measurements at $c \leq 0.1$ g/dl. Continuity between measurements carried out with the two μ -rheometers was assured by measuring η_0 and λ at $c = 0.1$ g/dl with both μ -rheometers. Black dashed line is the theoretical prediction of Eq. (3) with $\nu = 0.533$, derived from the data in (a). Red dotted line is the Zimm relaxation time measured through Eq. (2). Error bars falling within the symbol are not shown.

ν .^{42,45} The zero-shear viscosity has also been used as a rheological “biomarker” for the characterization of the protein solutions.^{4,5,67} Choi and Park,⁵ for instance, demonstrated that the folding and unfolding of protein solutions could be quantified through the

measurement of the zero-shear viscosity. The μ -rheometer could be used in similar studies and could potentially provide additional information regarding the link between protein folding and fluid elasticity^{68,69} due to the simultaneous measurement of both η_0 and λ .

Another advantage of the μ -rheometer is the very simple microfluidic setup, with a straight channel having a single inlet and a single outlet. Few other microfluidic rheometry platforms offer such simplicity; examples include the platform introduced by Hudson *et al.*⁴ and the iCapillary introduced by Solomon *et al.*⁷⁰ The iCapillary, however, could not easily measure zero-viscosity as the smallest shear rate applicable was $\dot{\gamma} = 1640 \text{ s}^{-1}$. The μ -rheometer can also be used for rheological characterization in parallel, assuming that independent pressure-pumps are available. This is a clear advantage over conventional rheometry where parallel analysis is possible only by using several rheometers in parallel. Additionally, the conventional rheometer cannot carry out simultaneous measurement of zero-shear viscosity and longest relaxation time, as the shear viscosity is measured imposing a continuous rotational flow, while the longest relaxation time λ is generally measured imposing an oscillatory flow.⁵⁰ Finally, the fact that measurements with the μ -rheometer require only a few microliters of sample (less than $100 \mu\text{l}$ in some cases) makes the μ -rheometer a potential gold standard for the characterization of rare and expensive biofluids.¹⁹

Despite clear advantages, the μ -rheometer also presents some limitations. The current setup does not allow measurements at different temperatures. Choi and Park⁵ inserted their experimental apparatus in an incubator to carry out measurements at different temperatures: this can be a possible solution for temperature controlled measurements in the μ -rheometer. Alternative methodologies are based on the integration of electrofluidic circuits²⁸ or localized temperature controlled circuits.⁷¹ Integration of the μ -rheometer with any system for localized temperature control would further reduce the gap between conventional and microfluidic rheometry. Another disadvantage is that measurements of Newtonian liquids (i.e., inelastic fluids with $\lambda = 0$) with experimental apparatus 2 are not possible, as the migration toward the channel centerline is driven by the elasticity of the suspending medium.^{35,36,53} Without elastic effects, particles do not migrate toward the channel centerline, and therefore, the measurement of the volumetric flow rate Q is not possible. However, by using experimental apparatus 1, the flow rate can be read and the viscosity can be evaluated, as for a conventional capillary rheometer.

The μ -rheometer cannot be used to measure the rheological properties of shear-thinning liquids because the theoretical curve introduced by Romeo *et al.*,⁵⁹ employed here for the simultaneous measurement of η_0 and λ , is valid only for second-order fluids. Under an experimental point of view, shear-thinning features promote transversal migration toward the channel walls.^{54–56} During the experiment, if particles are observed near the channel walls, it means that the suspending liquid presents significant shear-thinning features, and therefore, the μ -rheometer cannot be used. In addition, due to the working principle based on the transversal particle migration in homogeneous liquids, the μ -rheometer is not expected to work on heterogeneous systems such as emulsions or suspensions. The last two limitations could be potentially addressed in the future when (if) theoretical models for the description of particle

migration in shear-thinning liquids and heterogeneous systems will be available.

Probably, the most relevant disadvantage of the current μ -rheometer setup is the post-processing required before being able to determine the fluid properties. The problem is not the post-processing itself (which does not take longer than 10 min), rather the verification of the hypothesis underlying the measurement of the longest fluid relaxation time λ through Eq. (9). The measurement of λ , indeed, is accurate only when $\Theta < 1.4$, $De < 1$, and $Re < 1$. The evaluation of all the three dimensionless parameters depends on the imposed volumetric flow rate Q , on the longest relaxation time of the fluid λ , and on the normalized fraction of aligned particles f_1 . With experimental apparatus 1, the flow rate Q can be measured through the flow sensor, while λ and f_1 are actually the result of the post-processing. Therefore, it is only after the post-processing that the validity of the measured λ values can be verified. This issue is mitigated by the experience of the user performing the measurements, but some trial-error is required. A potential solution that deserves further investigation is the use of a real-time particle tracking software, such as that commercially available from Photometrics, based on the work by Sbalzarini and Koumoutsakos.⁷² In this way, the validity of the assumptions could be verified in real-time, and experimental conditions could be adjusted to obtain reliable and accurate values of λ . The measurement of the zero-shear viscosity η_0 remains possible using Eq. (6), as long as the confinement ratio for experimental apparatus 2 [Fig. 1(b)] is $\beta \lesssim 0.1$.

VI. CONCLUSIONS

In summary, I introduced the μ -rheometer, a microfluidic platform for the simultaneous measurement of zero-shear viscosity, and the longest relaxation time. The working principle of the μ -rheometer employed in this work was the same as that introduced in the original publication;¹⁸ however, herein the flow was imposed using a pressure pump instead of syringe pumps. This modification allowed for the simultaneous measurement of the zero-shear viscosity η_0 and the longest fluid relaxation time λ . Two sets of polyethylene oxide solutions in glycerol-water 25 wt.% (PG4) and pure water (P4) were characterized through conventional rheometry, and the results were compared to those derived through the μ -rheometer; good agreement was found between all the experimental data. A simpler and cheaper version of the μ -rheometer, i.e., without the flow sensor, was found to be accurate for the measurements of the rheological properties. Future integration with localized temperature systems^{28,71} and implementation of the real-time particle tracking algorithm are anticipated to further reduce the gap between conventional and microfluidic rheometry.

ACKNOWLEDGMENTS

The author acknowledges Professor Gaetano D'Avino for helpful comments and Dr. Dan Curtis for careful proofreading. The author acknowledges support from EPSRC New Investigator Award (Grant Ref. No. EP/S036490/1) and EPSRC Platform Grant (Grant Ref. No. EP/N013506/1).

DATA AVAILABILITY

The data that support the findings of this study are available from the corresponding author upon reasonable request.

REFERENCES

- ¹E. Dickinson, "Hydrocolloids at interfaces and the influence on the properties of dispersed systems," *Food Hydrocolloids* **17**, 25–39 (2003).
- ²I. W. Sutherland, "Novel and established applications of microbial polysaccharides," *Trends Biotechnol.* **16**, 41–46 (1998).
- ³C. Yan and D. J. Pochan, "Rheological properties of peptide-based hydrogels for biomedical and other applications," *Chem. Soc. Rev.* **39**, 3528–3540 (2010).
- ⁴S. D. Hudson, P. Sarangapani, J. A. Pathak, and K. B. Migler, "A microliter capillary rheometer for characterization of protein solutions," *J. Pharm. Sci.* **104**, 678–685 (2015).
- ⁵S. Choi and J.-K. Park, "Microfluidic rheometer for characterization of protein unfolding and aggregation in microflows," *Small* **6**, 1306–1310 (2010).
- ⁶J. Heinrich, L. Balleisen, H. Schulte, G. Assmann, and J. van de Loo, "Fibrinogen and factor VII in the prediction of coronary risk. Results from the PROCAM study in healthy men," *Arterioscler. Thromb.: J. Vasc. Biol.* **14**, 54–59 (1994).
- ⁷D. J. Cook, T. A. Hollowood, R. S. Linforth, and A. J. Taylor, "Oral shear stress predicts flavour perception in viscous solutions," *Chem. Senses* **28**, 11–23 (2003).
- ⁸M. S. Owens, M. Vinjamur, L. Scriven, and C. Macosko, "Misting of non-Newtonian liquids in forward roll coating," *J. Non-Newtonian Fluid Mech.* **166**, 1123–1128 (2011).
- ⁹D. Vlassopoulos and W. Schowalter, "Characterization of the non-Newtonian flow behavior of drag-reducing fluids," *J. Non-Newtonian Fluid Mech.* **49**, 205–250 (1993).
- ¹⁰J. Husny and J. J. Cooper-White, "The effect of elasticity on drop creation in T-shaped microchannels," *J. Non-Newtonian Fluid Mech.* **137**, 121–136 (2006).
- ¹¹A. Groisman and V. Steinberg, "Efficient mixing at low Reynolds numbers using polymer additives," *Nature* **410**, 905 (2001).
- ¹²M. Asghari, M. Serhatlioglu, B. Ortaç, M. E. Solmaz, and C. Elbuken, "Sheathless microflow cytometry using viscoelastic fluids," *Sci. Rep.* **7**, 12342 (2017).
- ¹³D. Dannhauser, G. Romeo, F. Causa, I. De Santo, and P. Netti, "Multiplex single particle analysis in microfluidics," *Analyst* **139**, 5239–5246 (2014).
- ¹⁴D. Dannhauser, D. Rossi, F. Causa, P. Memmolo, A. Finizio, T. Wriedt, J. Hellmers, Y. Eremin, P. Ferraro, and P. Netti, "Optical signature of erythrocytes by light scattering in microfluidic flows," *Lab Chip* **15**, 3278–3285 (2015).
- ¹⁵J. Nam, H. Lim, D. Kim, H. Jung, and S. Shin, "Continuous separation of microparticles in a microfluidic channel via the elasto-inertial effect of non-Newtonian fluid," *Lab Chip* **12**, 1347–1354 (2012).
- ¹⁶X. Lu and X. Xuan, "Continuous microfluidic particle separation via elasto-inertial pinched flow fractionation," *Anal. Chem.* **87**, 6389–6396 (2015).
- ¹⁷J. Zilz, C. Schäfer, C. Wagner, R. J. Poole, M. A. Alves, and A. Lindner, "Serpentine channels: Micro-rheometers for fluid relaxation times," *Lab Chip* **14**, 351–358 (2014).
- ¹⁸F. Del Giudice, G. D'Avino, F. Greco, I. De Santo, P. A. Netti, and P. L. Maffettone, "Rheometry-on-a-chip: Measuring the relaxation time of a viscoelastic liquid through particle migration in microchannel flows," *Lab Chip* **15**, 783–792 (2015).
- ¹⁹S. Gupta, W. S. Wang, and S. A. Vanapalli, "Microfluidic viscometers for shear rheology of complex fluids and biofluids," *Biomicrofluidics* **10**, 043402 (2016).
- ²⁰V. Sharma, A. Jaishankar, Y.-C. Wang, and G. H. McKinley, "Rheology of globular proteins: Apparent yield stress, high shear rate viscosity and interfacial viscoelasticity of bovine serum albumin solutions," *Soft Matter* **7**, 5150–5160 (2011).
- ²¹T. G. Mason and D. A. Weitz, "Optical measurements of frequency-dependent linear viscoelastic moduli of complex fluids," *Phys. Rev. Lett.* **74**, 1250 (1995).
- ²²T. G. Mason, "Estimating the viscoelastic moduli of complex fluids using the generalized Stokes-Einstein equation," *Rheol. Acta* **39**, 371–378 (2000).
- ²³M. Tassieri, "Microrheology with optical tweezers: Peaks and troughs," *Curr. Opin. Colloid Interface Sci.* **43**, 39 (2019).
- ²⁴M. Tassieri, F. Del Giudice, E. J. Robertson, N. Jain, B. Fries, R. Wilson, A. Gli-dle, F. Greco, P. A. Netti, P. L. Maffettone *et al.*, "Microrheology with optical tweezers: Measuring the relative viscosity of solutions 'at a glance'," *Sci. Rep.* **5**, 8831 (2015).
- ²⁵C. J. Pipe and G. H. McKinley, "Microfluidic rheometry," *Mech. Res. Commun.* **36**, 110–120 (2009).
- ²⁶S. Haward, "Microfluidic extensional rheometry using stagnation point flow," *Biomicrofluidics* **10**, 043401 (2016).
- ²⁷P. Arosio, K. Hu, F. A. Aprile, T. Müller, and T. P. Knowles, "Microfluidic diffusion viscometer for rapid analysis of complex solutions," *Anal. Chem.* **88**, 3488–3493 (2016).
- ²⁸T.-A. Lee, W.-H. Liao, Y.-F. Wu, Y.-L. Chen, and Y.-C. Tung, "Electrofluidic circuit-based microfluidic viscometer for analysis of Newtonian and non-Newtonian liquids under different temperatures," *Anal. Chem.* **90**, 2317–2325 (2018).
- ²⁹G. Vishwanathan and G. Juarez, "Steady streaming viscometry of Newtonian liquids in microfluidic devices," *Phys. Fluids* **31**, 041701 (2019).
- ³⁰S. Gupta and S. A. Vanapalli, "Microfluidic shear rheology and wall-slip of viscoelastic fluids using holography-based flow kinematics," *Phys. Fluids* **32**, 012006 (2020).
- ³¹K.-W. Hsiao, J. Dinic, Y. Ren, V. Sharma, and C. M. Schroeder, "Passive non-linear microrheology for determining extensional viscosity," *Phys. Fluids* **29**, 121603 (2017).
- ³²A. Shenoy, C. V. Rao, and C. M. Schroeder, "Stokes trap for multiplexed particle manipulation and assembly using fluidics," *Proc. Natl. Acad. Sci. U. S. A.* **113**, 3976–3981 (2016).
- ³³A. E. Koser, L. Pan, N. C. Keim, and P. E. Arratia, "Measuring material relaxation and creep recovery in a microfluidic device," *Lab Chip* **13**, 1850–1853 (2013).
- ³⁴A. M. Leshansky, A. Bransky, N. Korin, and U. Dinnar, "Tunable nonlinear viscoelastic 'focusing' in a microfluidic device," *Phys. Rev. Lett.* **98**, 234501 (2007).
- ³⁵S. Yang, J. Y. Kim, S. J. Lee, S. S. Lee, and J. M. Kim, "Sheathless elasto-inertial particle focusing and continuous separation in a straight rectangular microchannel," *Lab Chip* **11**, 266–273 (2011).
- ³⁶F. Del Giudice, G. Romeo, G. D'Avino, F. Greco, P. A. Netti, and P. L. Maffettone, "Particle alignment in a viscoelastic liquid flowing in a square-shaped microchannel," *Lab Chip* **13**, 4263–4271 (2013).
- ³⁷F. Del Giudice, V. Calcagno, V. Esposito Taliento, F. Greco, P. A. Netti, and P. L. Maffettone, "Relaxation time of polyelectrolyte solutions: When μ -rheometry steps in charge," *J. Rheol.* **61**, 13–21 (2017).
- ³⁸F. Del Giudice, S. J. Haward, and A. Q. Shen, "Relaxation time of dilute polymer solutions: A microfluidic approach," *J. Rheol.* **61**, 327–337 (2017).
- ³⁹F. Del Giudice, M. Tassieri, C. Oelschlaeger, and A. Q. Shen, "When microrheology, bulk rheology, and microfluidics meet: Broadband rheology of hydroxyethyl cellulose water solutions," *Macromolecules* **50**, 2951–2963 (2017).
- ⁴⁰A. Matsumoto, F. Del Giudice, R. Rotrattanadumrong, and A. Q. Shen, "Rheological scaling of ionic-liquid-based polyelectrolytes in ionic liquid solutions," *Macromolecules* **52**, 2759–2771 (2019).
- ⁴¹R. H. Ewoldt, M. T. Johnston, and L. M. Caretta, "Experimental challenges of shear rheology: How to avoid bad data," in *Complex Fluids in Biological Systems* (Springer, 2015), pp. 207–241.
- ⁴²M. Rubinstein, R. H. Colby *et al.*, *Polymer Physics* (Oxford University Press, New York, 2003), Vol. 23.
- ⁴³B. H. Zimm, "Dynamics of polymer molecules in dilute solution: Viscoelasticity, flow birefringence and dielectric loss," *J. Chem. Phys.* **24**, 269–278 (1956).
- ⁴⁴P.-G. De Gennes, *Scaling Concepts in Polymer Physics* (Cornell University Press, 1979).
- ⁴⁵R. H. Colby, "Structure and linear viscoelasticity of flexible polymer solutions: Comparison of polyelectrolyte and neutral polymer solutions," *Rheol. Acta* **49**, 425–442 (2010).
- ⁴⁶A. Jain, B. Dünweg, and J. R. Prakash, "Dynamic crossover scaling in polymer solutions," *Phys. Rev. Lett.* **109**, 088302 (2012).

- ⁴⁷K.-W. Hsiao, C. Sasmal, J. Ravi Prakash, and C. M. Schroeder, "Direct observation of DNA dynamics in semidilute solutions in extensional flow," *J. Rheol.* **61**, 151–167 (2017).
- ⁴⁸C. D. Young and C. E. Sing, "Simulation of semidilute polymer solutions in planar extensional flow via conformationally averaged Brownian noise," *J. Chem. Phys.* **151**, 124907 (2019).
- ⁴⁹P. E. Rouse, Jr., "A theory of the linear viscoelastic properties of dilute solutions of coiling polymers," *J. Chem. Phys.* **21**, 1272–1280 (1953).
- ⁵⁰C. W. Macosko and R. G. Larson, *Rheology: Principles, Measurements, and Applications* (Wiley, 1994).
- ⁵¹F. Del Giudice, F. Greco, P. A. Netti, and P. L. Maffettone, "Is microrheometry affected by channel deformation?," *Biomicrofluidics* **10**, 043501 (2016).
- ⁵²J. C. Crocker and D. G. Grier, "Methods of digital video microscopy for colloidal studies," *J. Colloid Interface Sci.* **179**, 298–310 (1996).
- ⁵³G. D'Avino, G. Romeo, M. M. Villone, F. Greco, P. A. Netti, and P. L. Maffettone, "Single line particle focusing induced by viscoelasticity of the suspending liquid: Theory, experiments and simulations to design a micropipe flow-focuser," *Lab Chip* **12**, 1638–1645 (2012).
- ⁵⁴F. Del Giudice, G. D'Avino, F. Greco, P. A. Netti, and P. L. Maffettone, "Effect of fluid rheology on particle migration in a square-shaped microchannel," *Microfluid. Nanofluid.* **19**, 95–104 (2015).
- ⁵⁵F. Del Giudice, S. Sathish, G. D'Avino, and A. Q. Shen, "From the edge to the center": Viscoelastic migration of particles and cells in a strongly shear-thinning liquid flowing in a microchannel," *Anal. Chem.* **89**, 13146–13159 (2017).
- ⁵⁶M. Villone, G. D'Avino, M. Hulsen, F. Greco, and P. Maffettone, "Particle motion in square channel flow of a viscoelastic liquid: Migration vs secondary flows," *J. Non-Newtonian Fluid Mech.* **195**, 1–8 (2013).
- ⁵⁷R. B. Bird, R. C. Armstrong, and O. Hassager, *Dynamics of Polymeric Liquids*, Fluid mechanics Vol. 1 (Wiley, 1987).
- ⁵⁸J. J. Higdon and G. Muldowney, "Resistance functions for spherical particles, droplets and bubbles in cylindrical tubes," *J. Fluid Mech.* **298**, 193–210 (1995).
- ⁵⁹G. Romeo, G. D'Avino, F. Greco, P. A. Netti, and P. L. Maffettone, "Viscoelastic flow-focusing in microchannels: Scaling properties of the particle radial distributions," *Lab Chip* **13**, 2802–2807 (2013).
- ⁶⁰D. Di Carlo, "Inertial microfluidics," *Lab Chip* **9**, 3038–3046 (2009).
- ⁶¹R. Powell and W. Schwarz, "Rheological properties of polyethylene oxide solutions," *Rheol. Acta* **14**, 729–740 (1975).
- ⁶²K. W. Ebagninin, A. Benchabane, and K. Bekkour, "Rheological characterization of poly(ethylene oxide) solutions of different molecular weights," *J. Colloid Interface Sci.* **336**, 360–367 (2009).
- ⁶³V. Tirtaatmadja, G. H. McKinley, and J. J. Cooper-White, "Drop formation and breakup of low viscosity elastic fluids: Effects of molecular weight and concentration," *Phys. Fluids* **18**, 043101 (2006).
- ⁶⁴W. W. Graessley, "Entangled linear, branched and network polymer systems—Molecular theories," in *Synthesis and Degradation Rheology and Extrusion* (Springer, 1982), pp. 67–117.
- ⁶⁵K. Kang, L. J. Lee, and K. W. Koelling, "High shear microfluidics and its application in rheological measurement," *Exp. Fluids* **38**, 222–232 (2005).
- ⁶⁶D. C. Montgomery and G. C. Runger, *Applied Statistics and Probability for Engineers* (John Wiley & Sons, 2010).
- ⁶⁷S. Amin, C. A. Rega, and H. Jankevics, "Detection of viscoelasticity in aggregating dilute protein solutions through dynamic light scattering-based optical microrheology," *Rheol. Acta* **51**, 329–342 (2012).
- ⁶⁸M. Carrion-Vazquez, A. F. Oberhauser, S. B. Fowler, P. E. Marszalek, S. E. Broedel, J. Clarke, and J. M. Fernandez, "Mechanical and chemical unfolding of a single protein: A comparison," *Proc. Natl. Acad. Sci. U. S. A.* **96**, 3694–3699 (1999).
- ⁶⁹F. Rico, A. Rigato, L. Picas, and S. Scheuring, "Mechanics of proteins with a focus on atomic force microscopy," *J. Nanobiotechnol.* **11**, S3 (2013).
- ⁷⁰D. E. Solomon, A. Abdel-Raziq, and S. A. Vanapalli, "A stress-controlled microfluidic shear viscometer based on smartphone imaging," *Rheol. Acta* **55**, 727–738 (2016).
- ⁷¹D. Lee, C. Fang, A. S. Ravan, G. G. Fuller, and A. Q. Shen, "Temperature controlled tensiometry using droplet microfluidics," *Lab Chip* **17**, 717–726 (2017).
- ⁷²I. F. Sbalzarini and P. Koumoutsakos, "Feature point tracking and trajectory analysis for video imaging in cell biology," *J. Struct. Biol.* **151**, 182–195 (2005).